Fabrication of devices featuring covalently linked MoS2–graphene heterostructures

Emilio M. Pérez, Manuel Vázquez Sulleiro, Aysegul Develioglu, Ramiro Quirós-Ovies, Lucía Martín-Pérez, Natalia Martín Sabanés, María Lourdes Gonzalez-Juarez, I. Jénnifer Gómez, Mariano Vera-Hidalgo, Víctor Sebastián, Jesús Santamaría, Enrique Burzurí

To cite this version

Copyright

Embargo

Fabrication of covalently linked MoS₂–graphene heterostructure devices

Manuel Vázquez Sulleiro[1], Aysegul Develioglu[1], Ramiro Quirós-Ovies[1,2], Lucía Martín-Pérez[1], Natalia Martín Sabanés[1], Maria Lourdes Gonzalez-Juarez[1], I. Jénnifer Gómez[3], Mariano Vera-Hidalgo[1], Víctor Sebastián[2,4], Jesús Santamaría[2,4,5], Enrique Burzurí[1,6,*], and Emilio M. Pérez[1,*]

E-mail: enrique.burzuri@imdea.org (ORCID: 0000-0001-7906-7192), emilio.perez@imdea.org (ORCID: 0000-0002-8739-2777)

[1]IMDEA Nanociencia C/Faraday 9 Ciudad Universitaria de Cantoblanco, 28049 Madrid, Spain.

[2]Instituto de Nanociencia y Materiales de Aragón (INMA), CSIC-Universidad de Zaragoza, 50009 Zaragoza, Spain.

[3]CEITEC Masaryk University Kamenice 5, 62500 Brno, Czech Republic.

[4]Department of Chemical and Environmental Engineering Universidad de Zaragoza Campus Rio Ebro, 50018 Zaragoza, Spain.

[5]Networking Research Center on Bioengineering, Biomaterials and Nanomedicine (CIBER-BBN), 28029 Madrid, Spain.

[6]Departamento de Física de la Materia Condensada and Condensed Matter Physics Center (IFIMAC), Universidad Autónoma de Madrid, 28049, Madrid, Spain

ABSTRACT:

The most widespread method for the synthesis of 2D–2D heterostructures is the direct growth of one material on top of the other. Alternatively, flakes of different materials can be manually stacked on top of each other. Both methods typically involve stacking 2D layers through van der Waals forces — such that these materials are often referred to as 'van der Waals heterostructures' — and

are carried out one crystal or one device at a time. Here, we describe the covalent grafting of 2H-MoS$_2$ flakes on graphene monolayers embedded in field-effect transistors. A bifunctional molecule was used that features a maleimide and a diazonium functional group, known to connect to sulfide- and carbon-based materials, respectively. MoS$_2$ flakes were first exfoliated, functionalized by reaction with the maleimide moieties, then anchored to graphene through the diazonium groups. This approach enabled the simultaneous functionalization of several devices. The electronic properties of the resulting heterostructure are shown to be dominated by the MoS$_2$–graphene interface.

The combination of nanomaterials is a promising approach towards materials made by design. In particular, the stack of different 2D materials has attracted enough attention to inaugurate a field of research: van der Waals heterostructures[1]. These are typically synthesised either by van der Waals epitaxy[2], or by deterministic placement of flake(s) of one material on top of the other[1,3,4,5,6,7]. Within 2D-2D van der Waals heterostructures, the combination of transition metal dichalcogenides (TMDCs) and graphene is a particularly active area of research, as the combination of the semiconducting properties of TMDCs with the high carrier mobility of graphene is particularly attractive for applications[8,9,10,11,12,13,14,15,16]. Several TMDC-TMDC heterojunctions have also been described[17,18,19]. Although these physical approaches have proven promising for the construction of high-performance devices, in all cases the 2D layers are relatively weakly bonded and can be taken apart in some solvents or thermal processes[20,21], plus it suffers from a complete lack of control over the interface between nanomaterials in terms of electronic communication, chemical nature, and interlayer distance.

In order to overcome these shortcomings, we decided to explore covalent chemistry as an alternative method for the connection of 2D materials, using a molecule with two anchor points. On one hand, we exploit the chemistry of maleimide described by our group to functionalize sulfide-based materials under mild conditions[22,23,24,25]. On the other hand, we use a diazonium salt[26,27,28], which is the most common method for the covalent modification graphene[29,30]. The solvents play a key role to activate a specific part of the molecule for the covalent anchoring.

RESULTS AND DISCUSSION

Functionalization and characterization of MoS$_2$

Liquid phase exfoliation (LPE) of bulk MoS$_2$ was performed using an ultrasonic probe (1h) in N-Methyl-2-pyrrolidone (NMP). Unexfoliated material was separated through centrifugation, yielding an olive-colour supernatant which was stable in the NMP suspension. This suspension was filtered,

and the resulting exfoliated pristine material (p-MoS$_2$) presented a 2H polymorphism, as confirmed by Raman spectroscopy with the characteristic modes of 2H-MoS$_2$ and UV-Vis extinction showing the characteristic excitonic transitions (Supplementary Fig. 1-3)[31]. The experimental X-ray diffraction (XRD) pattern of p-MoS$_2$ is in good agreement with the simulated data for hexagonal 2H-MoS$_2$ crystal phase (CDCC 1922046, Supplementary Fig. 4). The position of the (002) reflection in the exfoliated MoS$_2$ appears shifted to lower angles compared to the as-received material due to the slight increase in the interlayer distance along the c direction[32]. The analysis of AFM showed an average thickness of 14.7 $\pm$ 5.1 nm of exfoliated material (see Supplementary Fig. 5). Besides, p-MoS$_2$ showed a Raman shift of 4 cm^{-1} in the in-plane E$^1_{2g}$ and out-of-plane A$_{1g}$, compared to bulk MoS$_2$ due to the exfoliation process. To functionalize p-MoS$_2$, the suspended material was transferred to a dry CH$_3$CN solution of phenylmaleimide diazonium (**1**) and the mixture was vigorously stirred overnight in the absence of light, to prevent activation of the diazonium group (Figure 1a)[33]. The mixture was filtered, and the solid washed several times with CH$_3$CN to remove unreacted **1**. The effectiveness of the washing progress was verified by UV-Vis (Supplementary Fig. 6), confirming the absence of maleimide after three washes. Considering the rich reactivity of diazonium compounds[33,34,35], we also made sure that the diazonium group **1** remained stable under the maleimide-MoS$_2$ reaction conditions: 90% of the reagent was recovered from the washing solutions after the reaction, Nuclear Magnetic Resonance (NMR) spectroscopy and Fourier Transform Infrared Spectroscopy (FTIR) confirmed the presence of the diazonium group (Supplementary Fig. 7-8).

Aryl diazonium salts can also functionalize basal plane 2H-MoS$_2$ without any previous treatment[36,37]. In order to verify the stability of the diazonium group in the f-MoS$_2$, we explored the electrochemical activity of the suspensions by cyclic voltammetry (CV) (Supplementary Fig. 9-10). CV of f-MoS$_2$ exhibited a broad reduction peak with a maximum current of -0.19 µA at -0.55 V. This current peak is ascribed to the electron transfer between the diazonium group **1** anchored to the

MoS$_2$ surface and the GCE. The electrochemical reduction mechanism of **1** consists of generating an aryl radical in addition to the dinitrogen loss derived from the reduction of the diazonium salt. The aryl radical consequently forms a stable covalent C-C bond with the electrode surface (see Supplementary Fig. 11). A similar procedure was performed with *p*-MoS$_2$ observing no electrochemical activity. Thus, our preliminary electrochemical characterization supports the covalent C-S bonding formed between the maleimide moiety and the exfoliated MoS$_2$, and proves the accessibility and reactivity of the diazo group for post-synthetic routes.

FTIR of the MoS$_2$ sample functionalized (*f*-MoS$_2$) with **1** shows conclusive evidence of C-S bond formation (Figure 1b). The presence of the carbonyl stretch of the maleimide (1714 cm^{-1}) is only observed in the modified MoS$_2$ (1712 cm^{-1}). Moreover, the C-H bending mode of the alkene (black trace, 841 cm^{-1}) disappears after the reaction with MoS$_2$. Functionalized material showed a new band assigned to the new C-S bond generated (724 cm^{-1}), confirming the connection between the organic moiety and the material[23]. A control experiment where *p*-MoS$_2$ was subjected to the same reaction protocol in the absence of **1** did not show any of these spectroscopic features. Thermogravimetric analysis (Supplementary Fig. 12) showed clear differences between the functionalized and pristine material, mainly with a first weight loss from 240 ℃ to 340 ℃, which can be attributed to the decomposition of the organic molecule anchored to the MoS$_2$ (Supplementary Fig. 12, orange trace). The following reaction process, between 360 to 560 ℃, occurs due to the oxidation of MoS$_2$; a final pronounced drop from 630 ℃ to 780 ℃ is observed, where the total burning of the sample occurs. In addition, at 600 ℃ the weight loss difference between pristine material against *f*-MoS$_2$ is 5%. To further investigate the elemental composition and its chemical state, X-ray photoelectron spectroscopy (XPS) was performed. The elemental analysis survey (Table S1) showed in the case of *f*-MoS$_2$ the presence of N (1.3 %, N 1s, 400.6 eV), B (0.6%, B 1s, 194.6 eV) and F (2.4%, F 1s, 686.8 eV) with atomic ratios in good agreement with the chemical composition of the functionalizing moiety, suggesting the anchoring of the molecule to

the surface of the material, including the unreacted diazo group (Supplementary Fig. 13). Fitting the S 2p core level spectra we can observe the characteristic doublet feature in the p-MoS$_2$. In the case of f-MoS$_2$ the peak becomes broader and requires a new component usually assigned to the S-C new bond generated in the covalent functionalization of the MoS$_2$ (Supplementary Fig. 14-15)[23,38,39].

Raman spectroscopy measurements (λ_{exc} = 633 nm) revealed the stability of the 2H-polytype after the functionalization (Figure 1c and Supplementary Fig. 16 for further details). The main in-plane E^1_{2g} and out-of-plane A_{1g} Raman modes are clearly observed. Additional complex second order double resonant peaks at around 170, 460 and 600 cm^{-1} appear due to the resonant excitation condition[40,41,42], and decrease in intensity with respect to the A_{1g} mode upon functionalization. Suppression of the second order resonant modes in the functionalized MoS$_2$ can be attributed to alteration of the resonant conditions upon functionalization. Similarly, the decrease of the complex mode at 460 cm^{-1} (2LA(M)) has been used as a marker of functionalization of MoS$_2$ elsewhere[41]. Additional changes between the Raman spectra of pristine and functionalized MoS$_2$ are discussed in detail in the Supplementary Table S2. Surface-enhanced Raman spectroscopy (SERS) analysis provides further indication of functionalization. In particular, SERS spectra of maleimide molecules in comparison with pristine and functionalized MoS$_2$, reveal enhanced Raman bands in the f-MoS$_2$ sample (notably at 1372 and 1601 cm^{-1}) attributed to the succinimide molecules, which is absent in the case of p-MoS$_2$ (Supplementary Fig. 17).

Formation and characterization of the covalent heterostructure

The covalent functionalization of the maleimide onto the surface of MoS$_2$ with a diazonium group makes the f-MoS$_2$ a suitable material for grafting onto carbon-based materials[43,44]. To create the covalent heterostructure, a Si/SiO$_2$ substrate containing single-layer CVD-grown graphene (CVDG) was introduced in a suspension of f-MoS$_2$ in water at 35 °C. In order to avoid undesired precipitation of the sulfur material onto the surface, the substrate was positioned vertically. After reaction, the device was washed meticulously with water. As previously mentioned, fluorine atoms

were not present in the pristine material, while the f-MoS$_2$ showed quantifiable amounts of it. Evidence of the decomposition of the diazo group and its consequent reactivity after the generation of the radical was found in the residues of the heterostructure reaction. The residual dispersion was filtered after reaction and XPS analysis showed the total disappearance of fluorine atoms from the MoS$_2$ surface (Supplementary Fig. 18).

To confirm the covalent anchoring of the MoS$_2$ flakes, Raman spectroscopy was performed to track the transformation of sp^2 carbon atoms of the graphene to sp^3 as indication of formation of a new C-C bond. Figure 2a shows a statistical analysis of I_D/I_G band ratio over hundreds of points where MoS$_2$ flakes were found, observing a substantial increase of the I_D/I_G ratio from 0.05 ± 0.03 in the pristine CVDG to 0.13 ± 0.05 in the case of the covalent f-MoS$_2$/CVDG heterostructure. Besides, a 2D mapping of a representative graphene region (21 x 24 µm) where I_D/I_G ratio was analyzed in the same area, before (Supplementary Fig. 19) and after (Figure 2b) the reaction, showed a clear increase of the relative D band intensity in localized areas (Figure 2bi). The areas where the D band increases also show the presence of the $I_{A_{1g}}$ signals of the MoS$_2$ (Figure 2bii), corroborating the formation of the covalent f-MoS$_2$/CVDG heterostructure.

Electrical properties

In order to measure the electrical properties of the heterostructure, we have fabricated graphene field-effect transistors (FET) on Si/SiO$_2$ substrates. In short, Cr/Au source and drain pads are deposited on CVD graphene by mask-less optical lithography and subsequent electron-beam evaporation of metals. In a second lithography step, we expose sets of 10x10 µm and 5x5 µm graphene bridges between the electrodes by optical lithography. The non-exposed graphene is removed by oxygen plasma etching. The devices are finally annealed at 300 ºC for 8 hours to remove any remnant organic compounds from the fabrication. Additional details about the fabrication process are described in Methods section. Supplementary Fig. 20 shows an optical and

AFM image taken on a representative 10x10 µm-bridge device. The Raman spectra measured on different spots of the device show a low D band, indicative of a mostly defect-free graphene bridge before functionalization.

In a first functionalization step, a substrate containing tens of CVDG FETs was immersed in the *f*-MoS$_2$ water dispersion for two hours using the same reaction conditions already described. The devices were thereafter blown dried with nitrogen. After the reaction, a full characterization of the in situ generated *f*-MoS$_2$/CVDG FET can be observed in the Figure 2c. Optical microscopy showed the presence of bright flakes onto the surface of the graphene device. Raman mapping of the device with the relative intensities of I_D/I_G from graphene and $I_{A_{1g}}$ from the MoS$_2$ ratifies the covalent anchor of the flakes, due to the fact that, as mentioned above, the increase in the I_D/I_G is observed where the MoS$_2$ flakes are located. A zoom-in AFM and SEM images of the covalent heterostructure can be observed in Supplementary Fig. 21. The preference of the *f*-MoS$_2$ flakes to anchor onto the CVDG device instead of the SiO$_2$ substrate can be clearly observed, together with some residual attachment to the gold electrode in Supplementary Fig. 22[45]. A control experiment with pristine MoS$_2$, without chemical modification was carried out placing the suspension of MoS$_2$ on top of the graphene, observing no significant changes in the D band intensity.

Further evidence of the covalent functionalization is observed in electron transport measurements. Gate voltage characteristics (I_{sd}-V_g) are measured on the CVDG FETs before and after the functionalization with *f*-MoS$_2$. The Si substrate serves as back-gate electrode and the SiO$_2$ as dielectric insulator. All the measurements were performed under vacuum conditions (~ 10^{-6} mbar). In pristine CVDG devices, the typical Dirac cone of semi-metallic graphene appears centered at V_g = 35.5 V, as shown in Figure 3a (black trace). In addition, the cone is clearly asymmetric with significantly lower mobility for negative charge carriers. See Supplementary Fig. 23 for the full gate voltage window. Graphene is therefore initially p-doped by electron-withdrawer impurities, most

likely as a consequence of remnant adsorbates from the fabrication process, the CVD growth or charged impurities in the SiO_2 substrate, as described in the literature[29,46,47].

The gate trace measured in the f-MoS_2/CVDG FET (orange curve in Figure 3a) reveals a shift of the Dirac cone towards positive gate voltages (V_g = 43.5 V) after the functionalization. This could be due to an electron withdrawal mechanism during the formation of the aryl covalent bond[48] but also due to charge transfer from the diazonium molecules when physisorbed on graphene[29,49]. The diazonium molecule has a well-known electron-withdrawer nature[29,48,49]. Indeed, it could be expected that only a fraction of the diazonium molecules covalently bond to the MoS_2 flakes will participate in the covalent formation of the heterostructure with graphene. In particular, reactivity will be locally higher for those linkers close to corrugated regions in graphene[49], the edges or grain boundaries and n-doped puddles[29].

The shift of the Dirac cone is accompanied by a clear reduction of the current at the cone minimum (18% reduction), together with a broadening of the cone minimum. This trend is clearer in Figure 3b where the gate traces have been renormalized to the potential at the cone minimum (V_g - V_m). The current suppression in graphene is unambiguously associated to the disruption of the sp^2 hybridization into a sp^3 hybridization due to the formation of covalent bonds[48,50], in this case between the diazonium molecule and the graphene. This finding is consistent with the increment of the D band observed in the Raman measurements that also points to the formation of covalent bonds, as showed in Figure 2.

A second functionalization of the same device during two additional hours (f-MoS2/CVDG (++), pink curve in Figure 3) yields a further shift of the Dirac cone towards positive gate voltages (V_g = 57 V). The current at the cone minimum is further suppressed but in a lesser relative degree (4% reduction). This seems to indicate that the initial two hours functionalization are enough to promote covalent bonding in most of the available graphene spots with higher reactivity. Note that the

control samples where the devices are exposed to only the DI water solvent show no significant doping effect on graphene after annealing (see Supplementary Fig. 26). Besides, the charge carrier mobility does not change significantly after functionalization and covalent bond formation between f-MoS$_2$ and graphene. The hole mobility in the sample in Figure 3a stays around μ_h = 500 cm^{2}V^{-1}s^{-1} before and after the second f-MoS$_2$ functionalization. It actually slightly increases after the first functionalization, most likely as a consequence of the interaction with MoS$_2$, as seen in the Supplementary Figure 23 and has been previously reported[51]. Electron mobility is μ_e = 66 cm^{2}V^{-1}s^{-1} for pristine graphene and lays out of the gate window for functionalized devices. See Suplementary Figure 23 information for additional details. The same trend appears in 19 out of 22 (86 %) measured devices (see Supplementary Fig. 24 for additional examples). The degree of p-doping and suppression of the current at the minimum, and therefore the possible chemisorption/physisorption balance, shows minor fluctuations from device to device. See Supplementary Fig. 25 for detailed statistics.

The impact of the MoS$_2$ flake thickness on the properties of the covalent heterostructure is explored in an additional set of control samples. Thinner average of MoS$_2$ flakes were obtained by incrementing the number of rpm in the centrifugation method from 5000 (2744 g) to 6500 (4637 g). AFM analysis showed a 24% decrease on the height average of the flakes (see Supplemenary Fig 27). After the functionalization with **1,** the resultant f-MoS$_2$/CVDG devices, prepared as described before, show identical gate characteristics as those described for thicker flakes in Figure 3a: p-doping, a 20% current reduction at the cone minimum and a roughly preserved mobility. Electron transport in the heterostructure is therefore dominated by the linker and the MoS$_2$ layer (or few layers) in close proximity to the rest of the heterostructure. See details in Supplementary Fig. 28-29.

The emergence of a p-doping effect on graphene in the covalent heterostructure seems to indicate that the electron-withdrawing character of the linker is predominant over the typically electron-donor character of MoS$_2$ when combined with graphene. It could also indicate that the diazonium

linker acts as electronic spacer between graphene and MoS_2. To better understand the role of the two components, we have studied separately the effect of the bare MoS_2 flakes and the bare diazonium salt used as linker when they couple to graphene. Supplementary Fig. 30 shows the gate voltage characteristic of a representative device after dipping the substrate with the diazonium salt **1** for five minutes to obtain a functionalization degree comparable to the covalent heterostructure in Figure 3a. A stronger p-doping effect, a larger current suppression at the cone minimum (33%) and pronounced reduction of the hole mobility in comparison with the covalent heterostructure is observed. On the other hand, Figure 3c and d shows the gate trace of a representative pristine graphene FET and the same device after drop casting in DI water containing bare MoS_2 flakes (without diazonium linkers). The coverage is comparable to that in the covalent heterostructure (see Supplementary Figure 32). Four main fingerprints of the van der Waals heterostructure appear that are not observed in the covalent heterostructures. First, a clear shift to lower gate voltages indicates n-doping of graphene as a consequence of the interactions with MoS_2. Second, the mobility of the electron charge carriers increases. Third, the current at the cone minimum slightly increases. Finally, the cone at the tip becomes sharper. This trend is observed in 34 of 36 (94%) measured devices (see Supplementary Figure 33 for additional examples). Further coverage with pristine MoS_2 flakes shows a boost of these characteristics; stronger n-doping and higher mobility (See Supplementary Figure 34). A similar trend is observed by depositing p-MoS_2 directly onto pre-functionalized **1**-CVDG substrates to form p-MoS_2/**1**-CVDG stacks (see Supplementary Figure 30-31). These results show that both covalent connections in our strategy for the formation of the heterostack are necessary to form f-MoS_2/CVDG FETs where the electrical properties are dominated by the molecular interface.

Finally, we carried out preliminary photoresponsivity experiments by shining the heterostructure with an ultraviolet laser source (365 nm). The initial characterization shows a photoresponse similar to the one described for graphene/MoS_2 van der Waals heterostructures (Supplementary Fig. 35)[52].

The photoelectric properties are therefore preserved in this covalent analogue. Further studies will be necessary to understand the role of other dopants, light intensity and wavelength in the photoresponsivity of the covalent heterostructure.

CONCLUSION

In conclusion, we have connected MoS_2 and graphene in a 2D–2D covalent heterostructure. In particular, we use chemoselectivity concepts to design a bifunctional molecule with a maleimide group, reactive towards MoS_2 under mild nonaqueous conditions, and a diazonium derivative, that is activated in water towards reaction with graphene. We use this to connect MoS_2 flakes to several graphene FET devices simultaneously. We observe that the electronic properties of the functionalized devices are dominated by the chemical interface, resulting in p-doped devices in which the charge mobility is conserved after reaction, and the degree of doping can be controlled by increasing the degree of functionalization. Very recently, Samorí and co-workers have shown the potential of chemistry to improve the performance devices based on a single TMDC through covalent connection[53]. The results described here show how through a chemical approach, we can build functional 2D-2D heterostructures beyond van der Waals[54]. In particular, vertical covalent connection allows for control of the interlayer distance and its chemical nature. For instance, we envision that small conjugated molecules will facilitate communication between the 2D materials, while longer, sufficiently rigid and insulating molecules will help decouple the materials, mirroring what is commonly found in molecular materials[55,56]. Meanwhile, the presence of the molecular interface also brings an additional lever on the final properties of devices, beyond the intrinsic properties of the materials. For example, one can easily imagine using molecules with unpaired spins to add magnetic properties that might find use in spintronics[57].Finally, we also show that the chemical approach to 2D-2D heterostructures has the potential to produce a large number of functioning devices simultaneously.

Acknowledgements

Author Contributions

M.V.S., E.B. and E.M.P. conceived and designed experiments. M.V.S., R.Q.O. and M.V.H. synthesized compound **1**. M.V.S. and R.Q.O. exfoliated and functionalized the materials. M.V.S., R.Q.O., N.M.S., M.L.G.J. and I.J.G. carried out the chemical and structural characterization. A.D., L.M.P. and E.B. fabricated the nanodevices and performed the electrical measurements. V.S., J. S., E.B., and E.M.P. supervised research and directed data analysis. M.V.S., E.B. and E.M.P. wrote the manuscript, with contributions from all authors.

Competing Interests statement

The authors declare no competing interests.

Figures
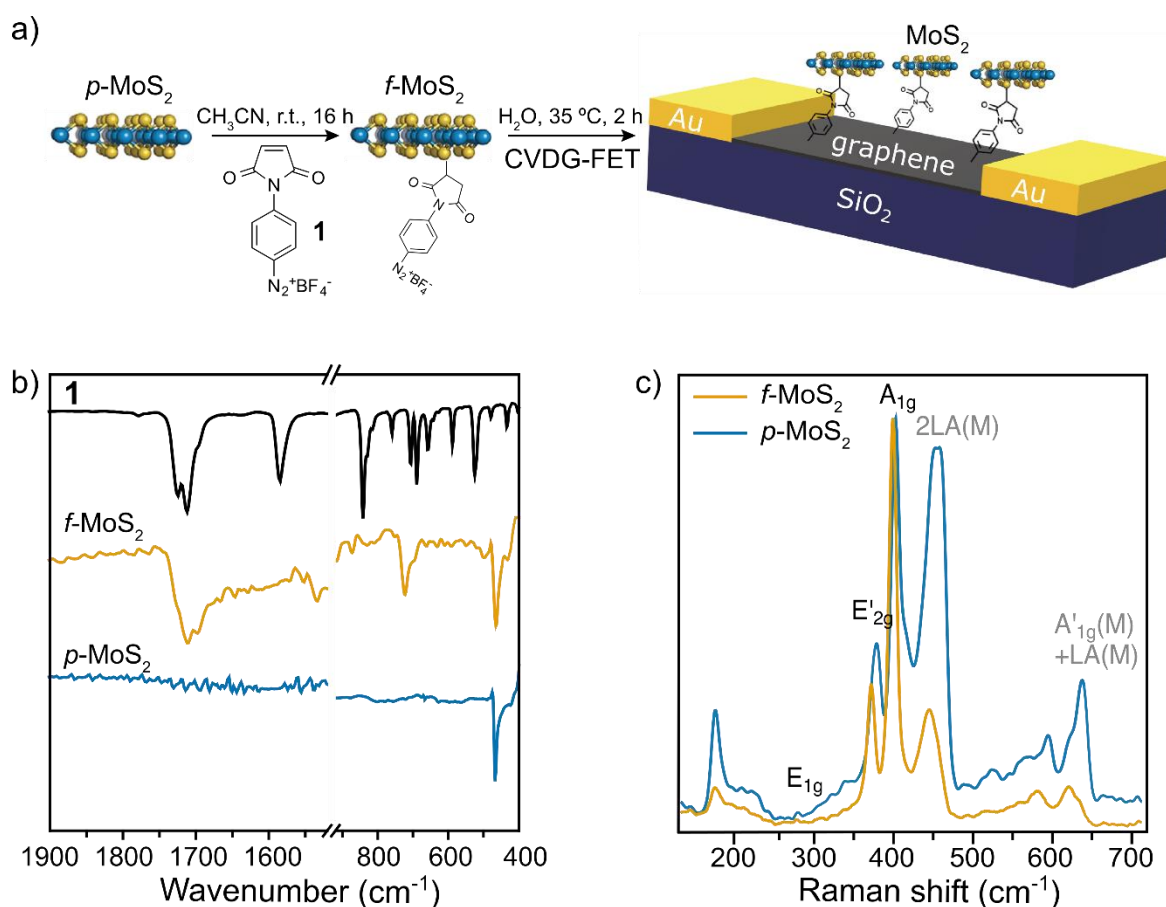
Figure 1. Schematic representation of the chemical approach to prepare the covalent *f*-MoS₂/CVDG FET heterostructure and characterization of *f*-MoS₂. a) Scheme of the covalent heterostructure formation. Firstly, the covalent functionalization of exfoliated MoS_2 (*p*-MoS₂) with phenylmaleimide diazonium **1**. Secondly, the anchoring of *f*-MoS₂ onto CVD Graphene FET device (*f*-MoS₂/CVDG). b) FTIR spectra of **1** (black trace), *f*-MoS₂ (orange trace) and *p*-MoS₂ (blue trace) where the appearance of a new band associated to the C-S bond is formed in the functionalized MoS_2 (724 cm⁻¹), as well as the presence of carbonyl stretch of the succinimide (1714 cm⁻¹). c) Raman spectra (λ_{exc} = 633 nm) of *f*-MoS₂ and *p*-MoS₂, the spectra show the characteristic E'₂g (in plane) and A₁g(out-of-plane) modes, as well as a second-order process peaks (LA(M)) with an overall reduction of intensity after the functionalization.
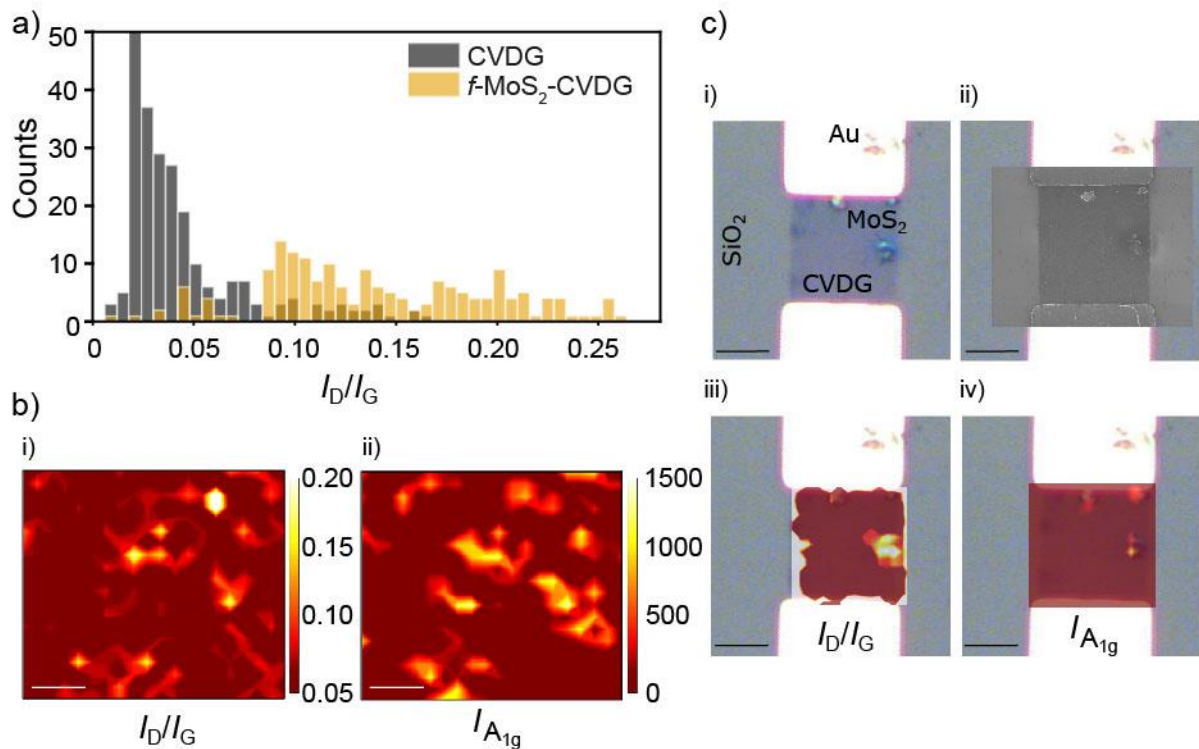
Figure 2. Characterization of the *f*-MoS₂/CVDG heterostructure. a) Histogram of the relative Raman intensities (I_D/I_G) of CVDG (before the reaction) and *f*-MoS₂/CVDG heterostructure (λ_{exc} 532 nm, N = >175), an increase of the ratio, confirming the covalent anchor, is observed after the functionalization. b) 2D Raman mapping of i) I_D/I_G (λ_{exc} 532 nm) and ii) I_{A1g} of MoS₂ (λ_{exc} 532 nm) of a 21 x 24 µm area of *f*-MoS₂/CVDG heterostructure, the locations where an increase of the I_D/I_G ratio is observed match with the $I_{A_{1g}}$ signals from the *f*-MoS₂. c) Characterization of *f*-MoS₂/CVDG FET device; the anchored MoS₂ flakes can be observed through i) Optical image and ii) SEM. iii) Raman mapping with the relative intensities of I_D/I_G and iv) $I_{A_{1g}}$ have a similar trend as described above. Scale bars of 5 µm.
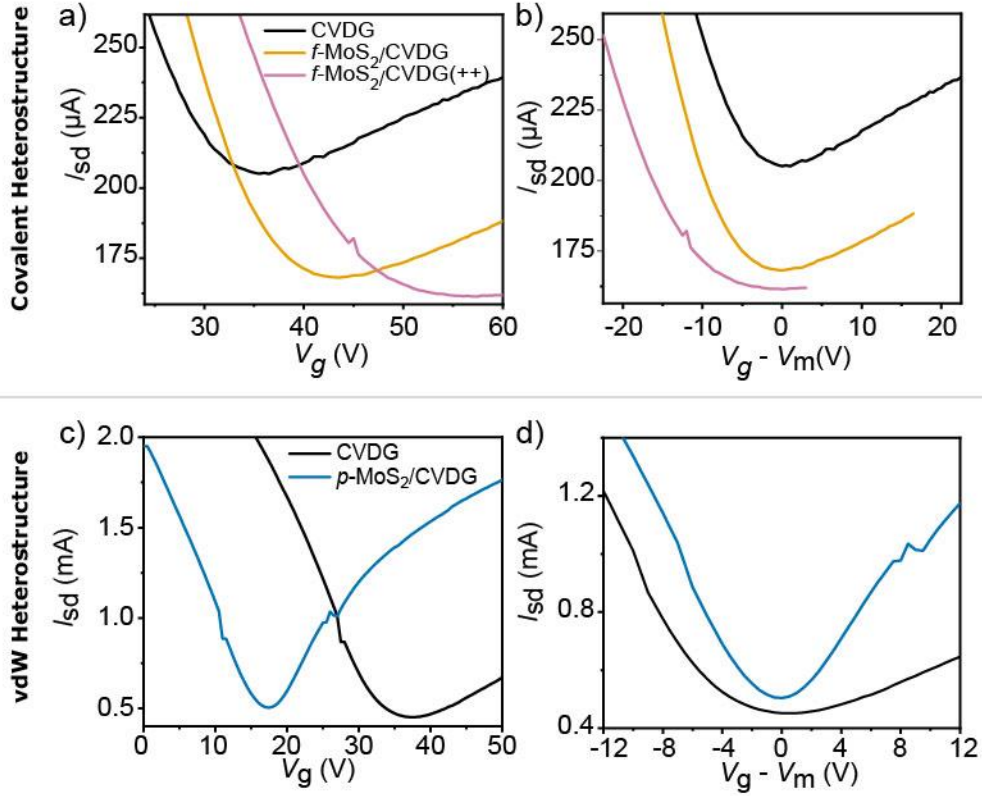
Figure 3. **Electrical properties of the covalent f-MoS$_2$/CVDG heterostructure and equivalent vdW heterostructure.** a) Gate voltage characteristics (I_{sd}-V_g) measured on a pristine CVDG-FET (black trace), the same device after two hours functionalization with f-MoS$_2$ (orange trace), and additional two hours functionalization ((f-MoS2/CVDG (++), pink trace). The measurement reveals a positive gate voltage shift of the Dirac cone and a reduction of the current caused by the anchor of the f-MoS$_2$. b) The same gate voltage characteristics renormalized to the V_g potential at the cone minimum V_m. c) Gate voltage characteristics (I_{sd}-V_g) measured on a pristine CVDG-FET (black trace) and the same device after generating the vdW heterostructure with p-MoS$_2$ (blue trace) with a device coverage comparable to the covalent heterostructure. The Dirac cone shifts to lower gate voltage and electron charge carriers mobility increases. d) The same gate voltage characteristics renormalized to the V_g potential at the cone minimum V_m.

References

1   Liu, Y. et al. Van der Waals heterostructures and devices. *Nat Rev. Mater.* **1**, 16042, (2016).

2   Robinson, J. A. Growing Vertical in the Flatland. *ACS Nano* **10**, 42-45, (2016).

3   Geim, A. K. & Grigorieva, I. V. Van der Waals heterostructures. *Nature* **499**, 419-425, (2013).

4   Yankowitz, M., Ma, Q., Jarillo-Herrero, P. & LeRoy, B. J. van der Waals heterostructures combining graphene and hexagonal boron nitride. *Nat. Rev. Phys.*, **1**, 112-125, (2019).

5   Neupane, G. P. et al. In-Plane Isotropic/Anisotropic 2D van der Waals Heterostructures for Future Devices. *Small* **15**, e1804733, (2019).

6   Novoselov, K. S., Mishchenko, A., Carvalho, A. & Castro Neto, A. H. 2D materials and van der Waals heterostructures. *Science* **353**, aac9439, (2016).

7   Jariwala, D., Marks, T. J. & Hersam, M. C. Mixed-dimensional van der Waals heterostructures. *Nat. Mater.* **16**, 170-181, (2017).

8   Bertolazzi, S., Krasnozhon, D. & Kis, A. Nonvolatile memory cells based on MoS2/graphene heterostructures. *ACS Nano* **7**, 3246-3252, (2013).

9   Ulstrup, S. et al. Ultrafast Band Structure Control of a Two-Dimensional Heterostructure. *ACS Nano* **10**, 6315-6322, (2016).

10   Shi, Y. et al. van der Waals epitaxy of MoS2 layers using graphene as growth templates. *Nano Lett.* **12**, 2784-2791, (2012).

11   Yu, L. et al. Graphene/MoS2 hybrid technology for large-scale two-dimensional electronics. *Nano Lett.* **14**, 3055-3063, (2014).

12   Lorchat, E. et al. Filtering the photoluminescence spectra of atomically thin semiconductors with graphene. *Nat. Nanotechnol.* **15**, 283-288, (2020).

13   Cao, Y. et al. Unconventional superconductivity in magic-angle graphene superlattices. *Nature* **556**, 43-50, (2018).

14   Kezilebieke, S. et al. Topological superconductivity in a van der Waals heterostructure. *Nature* **588**, 424-428, (2020).

15   Zhang, L. et al. Van der Waals heterostructure polaritons with moiré-induced nonlinearity. *Nature* **591**, 61-65, (2021).

16   Flöry, N. et al. Waveguide-integrated van der Waals heterostructure photodetector at telecom wavelengths with high speed and high responsivity. *Nat. Nanotechnol.* **15**, 118-124, (2020).

17   Wang, X. et al. Realization of vertical metal semiconductor heterostructures via solution phase epitaxy. *Nat. Commun.* **9**, 3611, (2018).

18   Le, C. T. et al. Effects of Interlayer Coupling and Band Offset on Second Harmonic Generation in Vertical MoS 2/MoS 2 (1-x) Se 2x Structures. *ACS Nano* **14**, 4366-4373, (2020).

19   Choi, W. et al. Optoelectronics of Multijunction Heterostructures of Transition Metal Dichalcogenides. *Nano Lett.* **20**, 1934-1943, (2020).

20   Li, C. et al. Engineering graphene and TMDs based van der Waals heterostructures for photovoltaic and photoelectrochemical solar energy conversion. *Chem. Soc. Rev.* **47**, 4981-5037, (2018).

21   Duong, D. L., Yun, S. J. & Lee, Y. H. van der Waals Layered Materials: Opportunities and Challenges. *ACS Nano* **11**, 11803-11830, (2017).

22   Vera-Hidalgo, M., Giovanelli, E., Navio, C. & Perez, E. M. Mild Covalent Functionalization of Transition Metal Dichalcogenides with Maleimides: A "Click" Reaction for 2H-MoS2 and WS2. *J. Am. Chem. Soc.* **141**, 3767-3771, (2019).

23   Quirós-Ovies, R. et al. Controlled Covalent Functionalization of 2H-MoS2 with Molecular or Polymeric Adlayers. *Chem. Eur. J.* **26**, 6629-6634 (2020).

24   Vázquez Sulleiro, M. et al. Covalent Cross-Linking of 2H-MoS2 Nanosheets. *Chem. Eur. J.* **27**, 2993-2996, (2021).

25   Villalva, J. et al. Covalent modification of franckeite with maleimides: connecting molecules and van der Waals heterostructures. *Nanoscale Horizons* **6**, 551-558, (2021).

26   Bahr, J. L. & Tour, J. M. Highly functionalized carbon nanotubes using in situ generated diazonium compounds. *Chem. Mater.* **13**, 3823-3824, (2001).

27   Strano, M. S. et al. Electronic structure control of single-walled carbon nanotube functionalization. *Science* **301**, 1519-1522, (2003).

28   Bahr, J. L. et al. Functionalization of carbon nanotubes by electrochemical reduction of aryl diazonium salts: a bucky paper electrode. *J. Am. Chem. Soc.* **123**, 6536-6542, (2001).

29   Paulus, G. L., Wang, Q. H. & Strano, M. S. Covalent electron transfer chemistry of graphene with diazonium salts. *Acc. Chem. Res.* **46**, 160-170, (2013).

30   Lomeda, J. R. et al. Diazonium Functionalization of Surfactant-Wrapped Chemically Converted Graphene Sheets. *J. Am. Chem. Soc.* **130**, 16201-16206, (2008).

31   Liu, Y., Zhao, Y., Jiao, L. & Chen, J. A graphene-like MoS 2/graphene nanocomposite as a highperformance anode for lithium ion batteries. *J. Mater. Chem. A* **2**, 13109-13115, (2014).

32   Yang, L. et al. Lattice strain effects on the optical properties of MoS2 nanosheets. *Sci. Rep.* **4**, 5649, (2014).

33   Mahouche-Chergui, S., Gam-Derouich, S., Mangeney, C. & Chehimi, M. M. Aryl diazonium salts: a new class of coupling agents for bonding polymers, biomacromolecules and nanoparticles to surfaces. *Chem. Soc. Rev.* **40**, 4143-4166, (2011).

34   Boukerma, K., Chehimi, M. M., Pinson, J. & Blomfield, C. X-ray photoelectron spectroscopy evidence for the covalent bond between an iron surface and aryl groups attached by the electrochemical reduction of diazonium salts. *Langmuir* **19**, 6333-6335, (2003).

35   Lomeda, J. R. et al. Diazonium functionalization of surfactant-wrapped chemically converted graphene sheets. *J. Am. Chem. Soc.* **130**, 16201-16206, (2008).

36   Chu, X. S. et al. Direct Covalent Chemical Functionalization of Unmodified Two-Dimensional Molybdenum Disulfide. *Chem. Mater.* **30**, 2112-2128, (2018).

37   Li, D. O., Chu, X. S. & Wang, Q. H. Reaction Kinetics for the Covalent Functionalization of Two-Dimensional MoS2 by Aryl Diazonium Salts. *Langmuir* **35**, 5693-5701, (2019).

38   Benson, E. E. et al. Balancing the hydrogen evolution reaction, surface energetics, and stability of metallic MoS2 nanosheets via covalent functionalization. *J. Am. Chem. Soc.* **140**, 441-450, (2018).

39   Chen, X. et al. Covalent Bisfunctionalization of Two-Dimensional Molybdenum Disulfide. *Angew. Chem. Int. Ed.* **60**, 13484-13492, (2021).

40   Fan, J.-H. et al. Resonance Raman scattering in bulk 2H-MX2 (M= Mo, W; X= S, Se) and monolayer MoS2. *J. Appl. Phys.* **115**, 053527, (2014).

41   Knirsch, K. C. et al. Basal-Plane Functionalization of Chemically Exfoliated Molybdenum Disulfide by Diazonium Salts. *ACS Nano* **9**, 6018-6030, (2015).

42   Mignuzzi, S. et al. Effect of disorder on Raman scattering of single-layer Mo S 2. *Phys. Rev. B* **91**, 195411, (2015).

43   Assresahegn, B. D., Brousse, T. & Bélanger, D. Advances on the use of diazonium chemistry for functionalization of materials used in energy storage systems. *Carbon* **92**, 362-381, (2015).

44   Bahr, J. L. & Tour, J. M. Highly functionalized carbon nanotubes using in situ generated diazonium compounds. *Chem. Mater.* **13**, 3823-3824, (2001).

45   Wang, Y. et al. Photoelectrochemical immunosensing of tetrabromobisphenol A based on the enhanced effect of dodecahedral gold nanocrystals/MoS2 nanosheets. *Sens. and Actuators B* **245**, 205-212, (2017).

46   Ryu, S. et al. Atmospheric oxygen binding and hole doping in deformed graphene on a SiO2 substrate. *Nano Lett.* **10**, 4944-4951, (2010).

47   Wang, Q. H. et al. Understanding and controlling the substrate effect on graphene electron-transfer chemistry via reactivity imprint lithography. *Nat. Chem.* **4**, 724-732, (2012).

48   Fan, X. Y., Nouchi, R., Yin, L. C. & Tanigaki, K. Effects of electron-transfer chemical modification on the electrical characteristics of graphene. *Nanotechnology* **21**, 475208, (2010).

49   Farmer, D. B. et al. Chemical doping and electron− hole conduction asymmetry in graphene devices. *Nano Lett.* **9**, 388-392, (2009).

50   Sinitskii, A. et al. Kinetics of diazonium functionalization of chemically converted graphene nanoribbons. *ACS Nano* **4**, 1949-1954, (2010).

51   Pham, T. et al. MoS2-graphene heterostructures as efficient organic compounds sensing 2D materials. *Carbon* **142**, 504-512, (2019).

52   Zhang, W. et al. Ultrahigh-gain photodetectors based on atomically thin graphene-MoS 2 heterostructures. *Sci. Rep.* **4**, 3826, (2014).

53   Ippolito, S., *et al.* Covalently interconnected transition metal dichalcogenide networks via defect engineering for high-performance electronic devices. *Nat. Nanotechnol.* **16,** 592–598 (2021).

54   Gbadamasi, S. et al. Interface chemistry of two-dimensional heterostructures–fundamentals to applications. *Chem. Soc. Rev.* **50**, 4684-4729 (2021).

55   Bottari, G., de la Torre, G., Guldi, D. M. & Torres, T. Covalent and Noncovalent Phthalocyanine−Carbon Nanostructure Systems: Synthesis, Photoinduced Electron Transfer, and Application to Molecular Photovoltaics. *Chem. Rev.* **110**, 6768-6816, (2010).

56   Martín, N. et al. Electronic Communication in Tetrathiafulvalene (TTF)/C60 Systems: Toward Molecular Solar Energy Conversion Materials? *Acc. Chem. Res.* **40**, 1015-1024, (2007).

57   Villalva, J. et al. Spin-state-dependent electrical conductivity in single-walled carbon nanotubes encapsulating spin-crossover molecules. *Nat. Commun* **12**, 1578, (2021).

Methods

Preparation of Liquid Phase Exfoliation MoS₂ (p-MoS₂). Liquid-Phase Exfoliation of MoS$_2$: 200 mg of MoS$_2$ powder and 200 mL of NMP were added in a round-bottom flask. The mixture was sonicated in a Vibracell 75115 (VC 505 / VC 750)-Bioshock Scientific. The Ultrasonic Processor was used during an hour, operating at the amplitude of 37%, without pulse at 2 ºC. Afterwards, the black dispersion was centrifuged for 30 minutes at 5000 rpm (Allegra X-15R Beckman Coulter centrifuge, FX6100 rotor, 20 ºC). Then, the supernatant (olive-color) was separated from the black sediment (non-exfoliated) by decanting and filtering with Omnipore 0.45 μm PTFE membrane filters, 45 mm in diameter. The membrane with the retained exfoliated MoS$_2$ was dispersed in acetonitrile and filtered again in order to clean the material. This re-dispersion process was repeated three times with 60 mL of acetonitrile and three times with 60 mL of isopropanol.

Functionalization of p-MoS₂ with N-(4-diazophenyl)maleimide. A 0.4 mg/mL dispersion of exfoliated MoS$_2$ is prepared by 10 seconds sonication of 8 mg of the material and 20 mL of dry acetonitrile in a glass vial. 1 mmol of *N*-(4-diazophenyl)maleimide was added to the dispersion and the mixture was stirred 16 hours at room temperature protected from the light. The resulting material was filtered with Omnipore 0.45 µm PTFE membrane filters (diameter of 25 mm) and washed three times with 40 mL of acetonitrile.

Fabrication of the field effect transistors. The fabrication of the graphene field-effect transistors involved two optical lithography steps. Initially, Si/SiO$_2$ wafers were cleaned using isopropanol and acetone to remove any traces of organic, ionic, and metallic impurities. Then, AZ1505 positive photoresist was spin coated at 5000 rpm for 1 min onto the surface followed by baking at 90ºC for 1 min to form a 450 nm resist layer. The electrodes and pads were defined by exposing the surface to UV light using a Heidelberg Instruments DWL66fs laser writer of 405nm (h-line) with 300 mJ/cm^2 dose. The pattern is subsequently developed with AZ-351B. Thereafter 5nm Cr and 80nm Au layers

were deposited using Ecovac e-beam evaporation by Angstrom Engineering. The source/drain electrodes are then obtained by lift-off. A second lithography step was carried out to etch graphene from unwanted areas and thus create a graphene channel between the electrodes. Negative photoresist AZ nLof 2070 was used to protect the graphene bridge between electrodes and the rest was exposed to oxygen plasma to etch. Finally, the resist was removed with acetone. Channel dimensions were set to 10x10μm and 5x5μm. The devices were annealed at 300 $^{\circ}$C for 8 hours after the fabrication.

Preparation of f-MoS$_2$/CVDG heterostructure. 1 mg of *f*-MoS$_2$ was dispersed in 10 mL of DI H$_2$O using a sonication bath for 10 minutes. Then CVDG-FET was vertically submerged held for 2h at 35 ºC in the absence of light. The resulting *f*-MoS$_2$/CVDG device was carefully washed with DI H$_2$O and flushed under N$_2$ flow. Same procedure was used for the *f*-MoS$_2$/CVDG FET heterostructure.

Data availability statement

The authors declare that all the data that support these findings are available in the manuscript, including its supporting information. Information files and from the corresponding authors upon request. Source data are provided with this paper.